High sensitivity and high Q-factor nanoslotted parallel quadrabeam photonic crystal cavity for real-time and label-free sensing

Daquan Yang, Shota Kita, Feng Liang, Cheng Wang, Huiping Tian, Yuefeng Ji, Marko Lonar, and Qimin Quan

Citation: Applied Physics Letters **105**, 063118 (2014); doi: 10.1063/1.4867254
View online: http://dx.doi.org/10.1063/1.4867254
View Table of Contents: http://scitation.aip.org/content/aip/journal/apl/105/6?ver=pdfcov
Published by the AIP Publishing

High sensitivity and high *Q*-factor nanoslotted parallel quadrabeam photonic crystal cavity for real-time and label-free sensing

Daquan Yang,[1,2,3] Shota Kita,[3] Feng Liang,[1] Cheng Wang,[3] Huiping Tian,[2] Yuefeng Ji,[2] Marko Lončar,[3] and Qimin Quan[1]
[1]*Rowland Institute at Harvard University, Cambridge, Massachusetts 02142, USA*
[2]*State Key Laboratory of Information Photonics and Optical Communications, School of Information and Communication Engineering, Beijing University of Posts and Telecommunications, Beijing 100876, China*
[3]*School of Engineering and Applied Sciences, Harvard University, Cambridge, Massachusetts 02138, USA*

(Received 16 September 2013; accepted 18 February 2014; published online 14 August 2014)

We experimentally demonstrate a label-free sensor based on nanoslotted parallel quadrabeam photonic crystal cavity (NPQC). The NPQC possesses both high sensitivity and high *Q*-factor. We achieved sensitivity (*S*) of 451 nm/refractive index unit and *Q*-factor >7000 in water at telecom wavelength range, featuring a sensor figure of merit >2000, an order of magnitude improvement over the previous photonic crystal sensors. In addition, we measured the streptavidin-biotin binding affinity and detected 10 ag/mL concentrated streptavidin in the phosphate buffered saline solution.
 [http://dx.doi.org/10.1063/1.4867254]

Real-time and label-free sensors are powerful tools to study protein dynamics. The figure of merit (FOM) of these sensors can be defined as $\mathrm{FOM} = S \cdot Q/\lambda_{res}$,[1] where $S = \Delta\lambda/\Delta n$ characterizes the shift of resonance ($\Delta\lambda$) in response to the surrounding index change (Δn), λ_{res} is the cavity resonance wavelength, and Q is the quality factor. Over the past several years, significant research has focused on achieving higher sensitivities or higher Q-factors in chip-integrated label-free biosensors based on different optical resonators,[2–4] such as surface plasmon resonance (SPR),[5–7] interferometry,[8–10] and optical cavities.[11–34] However, sensitivities (S) and quality factors (Q) have been trade-offs in label-free optical resonator sensors. For example, Lai *et al.*[22] demonstrated photonic crystal sensors with high Q-factors ~7000. However, S was limited to ~60 nm/RIU (refractive index unit), and FOM was ~300. Wang *et al.*[32] demonstrated large S of 900 nm/RIU in a slot double-beam waveguides/cavities. However, Q was limited to 700, and FOM was ~400. In the previous work,[33] we proposed and designed nanoslotted parallel quadrabeam photonic crystal cavity (NPQC) that can remedy the fundamental trade-off between high sensitivity and high Q-factor in cavity sensors. In this Letter, we report an experiment demonstration of sensitivity (S) of 451 nm/RIU, and Q-factor of 7015 in water at telecom wavelength range. This features FOM of 2060, an order of magnitude improvement over the previous photonic crystal sensors. In addition, we also report the detection of protein (streptavidin) in ultra-low concentration (detection limit ~10zM).

The NPQC devices used in this experiment were fabricated from silicon-on-insulator (SOI) with 220 nm device layer on a 2 μm thick buried oxide layer. First, electron beam (E-beam) lithography (Elionix ELS-7000) was performed using XR-1541 (6% HSQ) E-beam resist spun at 4000 rpm (~100 nm thick), followed by development in MF-319. Refractive ion etching of the exposed silicon region was performed with C_4F_8, SF_6, and Ar gases. Then, a second E-beam lithography was performed with SU8-2002 E-beam resist to fabricate the input/output bus waveguides.[35] Last, to remove the XR-1542 E-beam resist on the sensor, an opening was defined by photolithography with S1818 photoresist. 7:1 buffered oxide etchant (BOE) was applied for 1 min, followed by rinsing in deionized (DI) water. Finally, photoresist was removed with acetone and IPA.

Fig. 1(a) shows the scanning electron microscope (SEM) images of NPQC. It consists of four parallel photonic crystal nanobeam cavities with nano-gap separations. As designed in Ref. 33, gratings are in rectangular shape (Fig. 1(a), inset), the thickness of the cavity is 220 nm, the periodicity $a = 500$ nm, the nanobeam width $b = 200$ nm, the gap w between adjacent nanobeams is 100 nm, and the total width of the NPQC is 1.1 μm. The widths of the rectangular gratings are kept the same at 140 nm. The lengths of the gratings are quadratically tapered from cavity center $w_{cen} = 300$ nm to both sides $w_{side} = 225$ nm,

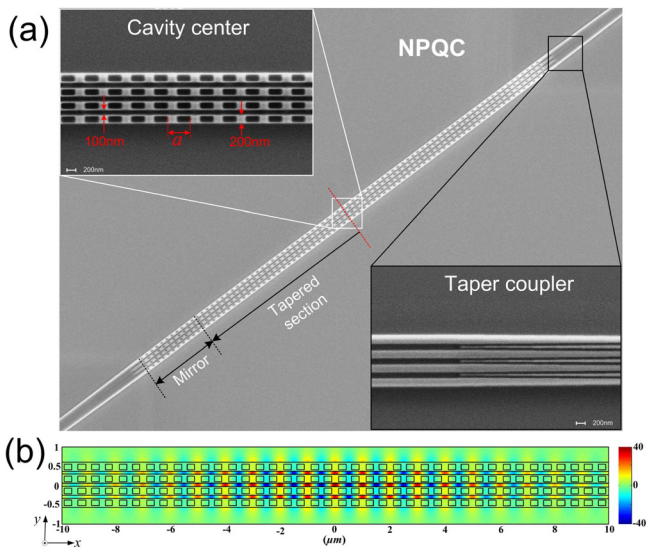

FIG. 1. (a) SEM images of the proposed Si-PhC NPQC cavity with the designed parameters: periodicity $a = 500$ nm, the nanobeam width $b = 200$ nm, the slot width w between adjacent nanobeams is 100 nm. The structure is symmetric with respect to its center (red dashed line). Inset: zoom in of the NPQC cavity center and taper couplers. (b) 3D FDTD simulation of the major field distribution profile (Ey) in the NPQC.

i.e., $w_x(i) = w_x(1) + (i-1)^2(w_x(i_{max}) - w_x(1))/(i_{max}-1)^2$ (i increases from 1 to i_{max}). The final cavity structure is symmetric to its center, and on each side, there are 40 gratings ($i_{max} = 40$) in the Gaussian mirror region and an additional 20 segments on both ends. Fig. 1(b) shows the field profile. It is clearly seen that optical field is strongly localized in the slotted region.

A schematic of the measurement setup is shown in Fig. 2(a). Light from a tunable laser (Santec TSL-510) was coupled to the edge of the chip with an optical fiber (OZ optics) through a polarizer controller. The SU8 polymer waveguide couplers fabricated on-chip were designed to match the mode of the tapered fiber.[35] Thus, light was effectively coupled from the optical fiber in-to NPQC, and out-to a second fiber and to the detector. A microfluidic channel was fabricated with Polydimethylsiloxane (PDMS) by replica molding of a SU8 template, with dimensions 2 mm × 100 μm × 50 μm (length, width, and height). Two sub-millimeter diameter holes were punched into PDMS as inlet and outlet for sample delivery. As shown in Fig. 2(b), microfluidic chip was held in place, on top of Si photonic chip, using home-made clamp. Figure 2(c) shows the experimental signal (top) and finite-difference time-domain simulation (FDTD) (bottom) of the NPQC immersed in DI water, respectively. The cavity has a resonance at 1536.30 nm, with Q factor of 7015, obtained from Lorentzian fitting (Fig. 2(c)). The experimental Q is lower than its theoretical prediction ($Q \sim 10^6$ at 1535.88 nm), primarily because of the water absorption at telecom wavelength range, surface roughness, and parameter discrepancy between the designed structure and final structure after Ebeam lithography and reactive ion etching processes. The water absorption will limit Q of the cavity to the order of 10^4.[36]

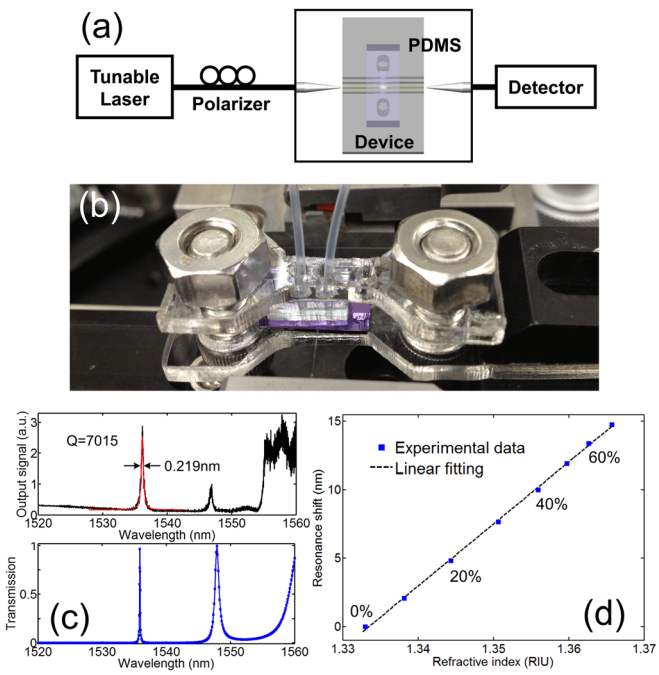

FIG. 2. (a) Schematics of the measurement setup. (b) Sensor chip with connected tubes clamped by home-made clamp and aligned to optical fibers. (c) Experimental signal (top) and FDTD simulated transmission spectrum (bottom) of the silicon NPQC immersed in distilled water, respectively. The Lorentzian fit to the resonance of the fundamental mode (1536.30 nm) indicates an experimentally measured Q-factor 7015 in water. (d) Resonant wavelength shifts as a function of the variations in refractive indices of different concentrations ethanol/water solutions (v/v).

Prior to protein detection experiments, NPQC sensor was calibrated with liquids of known refraction indices to characterize its response to bulk refractive index change. Different concentrations of ethanol/water solution were injected into the microfluidic channel. Fig. 2(d) shows the resonance shifts as a function of the refractive indices controlled by different volume ratios of ethanol and water. The volume ratios (v/v) used in our measurement are 0% (DI-water), 10%, 20%, 30%, 40%, 50%, 60%, 80%, respectively. As seen from Fig. 2(d), the dependence of the resonant shift on the refractive indices is linear and yields the experimental bulk refractive index sensitivity $S = \Delta\lambda/\Delta n = 451\,\text{nm/RIU}$, which is close to the FDTD simulation result (540 nm/RIU). Therefore, FOM is 2060. In addition, the sensitivity can be even increased by suspending the cavity off the substrate.

Next, NPQC sensor was used to detect streptavidin and quantify its affinity to biotin. The surface of the sensor was activated by oxygen plasma for 1 min, followed by a 10 min immersion in 95% aminopropyltriethoxysilane (APTES) in ethanol. The chip was then placed on a 80 °C heater for 2 h. Then, PDMS microfluidic channel was assembled on top of the sensor chip using the home-made clamp (Fig. 2(b)). Then, biotin in dimethylformamide (DMF) solution (1.0 mg/ml in DMF) was injected into the sensor chip with syringe pump. The chip was incubated for over 2 h, followed by flushing with phosphate buffered saline (PBS 1×) before the sensor was ready to do streptavidin experiment.

Streptavidin of varying concentrations was prepared by serially diluting streptavidin from 100 pg/mL down to 1 ag/mL in 1× PBS. The pure PBS solution was first injected by syringe pump (25 μL/min) into the sensor and a reference spectrum was taken as baseline. Streptavidin solutions were then injected from low-concentration to high-concentration. Measurements of the NPQC resonance were taken every 10 s, for 20 min, before the next concentration was introduced. In between two different concentrations, pure PBS solution was flushed for 4 min (PBS-wash). The resonance shift during the entire experiment is shown in real-time in Fig. 3. The vertical dotted purple line represents the time when the next concentration of streptavidin solution or pure-PBS was injected. Distinctive resonance shifts occurred at concentration of 10 ag/mL–100 ag/mL. At higher concentrations, resonance wavelengths exhibit saturation, indicating that available biotin coated on the sensor surface has been fully captured by streptavidin.[27,37] Inset of Fig. 3 shows the resonance shift vs. streptavidin concentration, both experiment data, and the fitting curve with Langmuir equation[28] $\Delta\lambda = C \cdot K_a \cdot \Delta\lambda_{max}/(1 + C \cdot K_a)$, where C is the streptavidin concentration and K_a is the affinity constant. From fitting, we obtained $K_a = 2.50 \times 10^{18}\,\text{M}^{-1}$. This value is on the same order of magnitude with the streptavidin-biotin affinity measurement in water with microcavity,[34] but larger than the typical avidin-biotin affinity value ($10^{15}\,\text{M}^{-1}$).[28] We have repeatedly obtained this result with our sensors. Our hypothesis is that the difference is due to the effective concentration in the microfluidic channel being larger than the injected solution, or possibly due to the difference of streptavidin-biotin

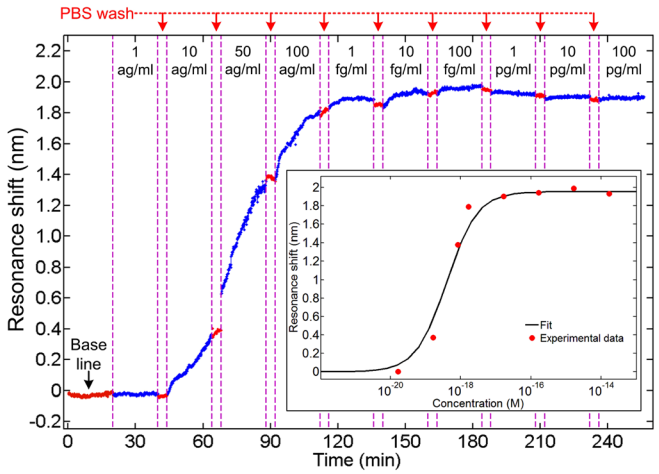

FIG. 3. Real time measurement of streptavidin/biotin binding showing shifts in cavity resonance wavelength (based on Lorentzian fit). Inset: resonance shift as a function of streptavidin concentration in PBS. (Experiments and fitted curve with Langmuir equation.)

affinity in the macro- and micro-environment. Further studies on this issue is being carried out. The lowest detected concentration in our experiment was ~200zM (10 ag/mL). The lowest detectable resonance shift can be derived from the fluctuation of the baseline in Fig. 3 ($\delta\lambda \sim 50$pm). Therefore, the detection limit of NPQC sensor is ~10zM, calculated from $K_a^{-1} \cdot \delta\lambda/(\delta\lambda_{max} - \delta\lambda)$.

In summary, we experimentally demonstrated NPQC label-free sensor with high sensitivity (451 nm/RIU) and high Q-factor (7015) at the same time, improving the sensor FOM (2060) by an order of magnitude over the previous photonic crystal sensors. We also reported the detection of streptavidin at ultra-low concentrations (10 ag/mL). Furthermore, the photonic crystal cavities can be easily multiplexed on chip, forming networks, and achieving high-throughput screening applications. The SOI platform also opens the door to the cost-effective mass production, highly promising for point-of-care medical diagnostics.

This research was supported by the Rowland Institute at Harvard. Device fabrication is performed at the Center for Nanoscale Systems (CNS) at Harvard. D. Yang acknowledges Dr. Yuan Lu for the discussions on the device fabrication. D. Yang acknowledges the support by National Natural Science Foundation of China (No. 61372038), National 973 Program (No. 2012CB315705), and BUPT Excellent Ph.D. Students Foundation (CX201212, CX201331), P. R. China. D. Yang thanks the China Scholarship Council (CSC) (No. 201206470026) for fellowship support. M. Loncar acknowledges support by the AFOSR Award FA9550-09-1-0669-DOD35CAP.

[1]L. J. Sherry, S. Chang, G. C. Schatz, and R. P. Van Duyne, Nano Lett. **5**, 2034–2038 (2005).
[2]X. Fan, I. M. White, S. I. Shopova, H. Zhu, J. D. Suter, and Y. Sun, Anal. Chim. Acta **620**, 8–26 (2008).
[3]C. A. Barrios, M. Banuls, V. G.-Pedro, K. B. Gylfason, B. Sanchez, A. Griol, A. Maquieira, H. Sohlstrom, M. Holgado, and R. Casquel, Opt. Lett. **33**, 708–710 (2008).
[4]H. K. Hunt and A. M. Armani, Nanoscale **2**, 1544–1559 (2010).
[5]J. N. Anker, W. P. Hall, O. Lyandres, N. C. Shah, J. Zhao, and R. P. Duyne, Nat. Mater. **7**, 442–453 (2008).
[6]R. Karlsson, J. Mol. Recognit. **17**, 151–161 (2004).
[7]C. Caucheteur, Y. Shevchenko, L. Shao, M. Wuilpart, and J. Albert, Opt. Express **19**, 1656–1664 (2011).
[8]J. Yang, L. Jiang, S. Wang, B. Li, M. Wang, H. Xiao, Y. Lu, and H. Tsai, Appl. Opt. **50**, 5503–5507 (2011).
[9]A. Ymeti, J. Greve, P. V. Lambeck, T. Wink, S. van Hovell, T. A. M. Beumer, R. R. Wijn, R. G. Heideman, V. Subramaniam, and J. S. Kanger, Nano Lett. **7**, 394–397 (2007).
[10]A. Ymeti, J. S. Kanger, J. Greve, G. A. Besselink, P. V. Lambeck, R. Wijn, and R. G. Heideman, Biosens. Bioelectron. **20**, 1417–1421 (2005).
[11]F. Vollmer and S. Arnold, Nat. Methods **5**, 591–596 (2008).
[12]C. Kang and S. M. Weiss, Opt. Express **16**, 18188–18193 (2008).
[13]D. Psaltis, S. R. Quake, and C. Yang, Nature **442**, 381–386 (2006).
[14]M. Loncar, A. Scherer, and Y. Qiu, Appl. Phys. Lett. **82**, 4648–4651 (2003).
[15]E. Chow, A. Grot, I. W. Mirkarimi, M. Sigalas, and G. Girolami, Opt. Lett. **29**, 1093–1095 (2004).
[16]T. Xu, N. Zhu, M. Y.-C. Xu, L. Wosinski, J. Stewart Aitchison, and H. E. Ruda, Opt. Express **18**, 5420–5425 (2010).
[17]F. Fan, W. Gu, X. Wang, and S. Chang, Appl. Phys. Lett. **102**, 121113 (2013).
[18]Q. Quan, I. B. Burgess, S. K. Y. Tang, D. L. Floyd, and M. Loncar, Opt. Express **19**, 22191–22197 (2011).
[19]C. Kang, C. T. Phare, Y. A. Vlasov, S. Assefa, and S. M. Weiss, Opt. Express **18**, 27930–27937 (2010).
[20]D. Yang, H. Tian, and Y. Ji, Opt. Express **19**, 20023–20034 (2011).
[21]Q. Quan, D. L. Floyd, I. B. Burgess, P. B. Deotare, I. W. Frank, S. K. Y. Tang, R. Ilic, and M. Loncar, Opt. Express **21**(26), 32225–32233 (2013).
[22]W. Lai, S. Chakravarty, Y. Zou, Y. Guo, and R. T. Chen, Appl. Phys. Lett. **102**, 041111 (2013).
[23]J. L. Briscoe, S. Cho, and I. Brener, Opt. Lett. **38**, 2569–2571 (2013).
[24]F. DellOlio and V. M. N. Passaro, Opt. Express **15**, 4977–4993 (2007).
[25]S. Kita, S. Hachuda, K. Nozaki, and T. Baba, Appl. Phys. Lett. **97**, 161108 (2010).
[26]J. Jagerska, H. Zhang, Z. Diao, N. Le Thomas, and R. Houdre, Opt. Lett. **35**, 2523–2525 (2010).
[27]M. G. Scullion, A. Di Falco, and T. F. Krauss, Biosens. Bioelectron. **27**, 101–105 (2011).
[28]S. Zlatanovic, L. W. Mirkarimi, M. M. Sigalas, M. A. Bynum, E. Chow, K. M. Robotti, G. W. Burr, S. Esener, and A. Grot, Sens. Actuators, B **141**, 13–19 (2009).
[29]S. Pal, E. Guillermain, R. Sriram, B. L. Miller, and P. M. Fauchet, Biosens. Bioelectron. **26**, 4024–4031 (2011).
[30]S. Chakravarty, Y. Zou, W. Lai, and R. T. Chen, Biosens. Bioelectron. **38**, 170–176 (2012).
[31]A. Di Falco, L. OFaolain, and T. F. Krauss, Appl. Phys. Lett. **94**, 063503 (2009).
[32]B. Wang, M. A. Dundar, R. Ntzel, F. Karouta, S. He, and R. W. Heijden, Appl. Phys. Lett. **97**, 151105 (2010).
[33]D. Yang, H. Tian, Y. Ji, and Q. Quan, J. Opt. Soc. Am. B **30**, 2027–2031 (2013).
[34]S. Hachuda, S. Otsuka, S. Kita, T. Isono, M. Narimatsu, K. Watanabe, Y. Goshima, and T. Baba, Opt. Express **21**, 12815–12821 (2013).
[35]Q. Quan, P. B. Deotare, and M. Loncar, Appl. Phys. Lett. **96**(20), 203102 (2010).
[36]A. M. Armani and K. J. Vahala, Opt. Lett. **31**, 1896–1898 (2006).
[37]C. F. Carlborg, K. B. Gylfason, A. Kazmierczak, F. Dortu, M. J. Banuls Polo, A. M. Catala, G. M. Kresbach, H. Sohlstrom, T. Moh, L. Vivien, J. Popplewell, G. Ronan, C. A. Barrios, G. Stemme, and W. Wijngaart, Lab Chip **10**, 281–290 (2010).